FREQUENCY ESTIMATION OF RADAR SIGNALS USING AN ACOUSTO-OPTIC SPECTRUM ANALYZER AS AN RESM RECEIVER

by

Guy Farley

DEFENCE RESEARCH ESTABLISHMENT OTTAWA
TECHNICAL NOTE 88-15

Canada

JUNE 1988
Ottawa

National Defence / Défense nationale

FREQUENCY ESTIMATION OF RADAR SIGNALS USING AN ACOUSTO-OPTIC SPECTRUM ANALYZER AS AN RESM RECEIVER

by

Guy Farley
RESM Section
Electronic Warfare Division

DEFENCE RESEARCH ESTABLISHMENT OTTAWA
TECHNICAL NOTE 88-19

PCN
011LB11

JUNE 1988
OTTAWA

ACKNOWLEDGEMENT

The author wishes to thank Mr. Brian Kozminchuck for his conscientious review of this report and his helpful suggestions to enhance its clarity.

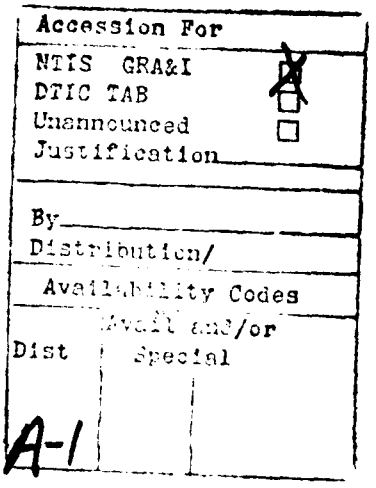

ABSTRACT

In this report we present a statistical model for the signals of an acousto-optic spectrum analyzer (AOSA). Using this model, we calculate the Cramér-Rao bound for the estimation of the carrier frequency of radar signals and the performance of the peak detector estimator. We also present an algorithm for sidelobe rejection.

RÉSUMÉ

Ce rapport présente un modèle statistique pour les signaux d'un analyseur de spectre acouto-optique. A partir de ce dernier, on y calcule la limite Cramér-Rao pour l'estimation de la fréquence des signaux radar ainsi que la performance d'un algorithme basé sur la détection d'un pic local. On y présente aussi un algorithme pour le rejet des lobes adjacents.

TABLE OF CONTENTS

LIST OF FIGURES

1.0 INTRODUCTION

It is expected that the Radar Electronic Support Measures (RESM) systems of the future will be exposed to extremely dense electromagnetic environments. Peak data rates from 500 thousand to one million pulses per second have been postulated for future scenarios [1]. This implies that the simultaneous arrival of different radar pulses will likely be frequent. However, conventional receivers using the Instantaneous Frequency Measurement technique tend to make erroneous measurements and miss signals when this occurs. This situation has prompted interest in channelized receivers which are able to measure the frequency of different radar signals that are simultaneously present at the front end of the receiver.

The acousto-optic spectrum analyzer (AOSA) is a viable contender among the general class of channelized receivers for use in future RESM environments and its frequency measurement performance is investigated in this report. In the next section, we present a model for the signals produced by the AOSA and in the third section we present the Cramér-Rao [9] bound for this problem. In the fourth section, we present the performance of a practical estimator for this problem, namely the peak detector estimator. And finally, in the fifth section we present a simple solution to the sidelobe rejection problem which might arise in certain cases where we apply the peak detector estimator.

2.0 MODEL

This section presents a model for the signal and the noise at the output of the AOSA which will form the basis of the performance analysis in the rest of the report. The first part presents a frequently used model for the configuration considered in this report and the second part discusses some of the reasons for assuming that additive Gaussian noise is a reasonable model of the corruption of the signal to be processed.

2.1 Signal

A block diagram of the AOSA configuration considered in this report is shown in Figure 1. The collimated light wave generated by the laser impinges on the Bragg cell at the Bragg angle θ_B. The diffracted field distribution in the frequency plane contains the frequency analysis of the input signal. Therefore, an array of photodetectors placed at the frequency plane can be used to transform the result of this analysis, which is in the form of optical signals, into electrical signals which can be further processed and analyzed. The input signal, which is typically an electrical signal from an antenna feed, is transformed by the Bragg cell to an acoustic wave which interacts with the optical beam with the result that part of the light entering the cell is diffracted at an angle proportional to the frequency of the input signal.

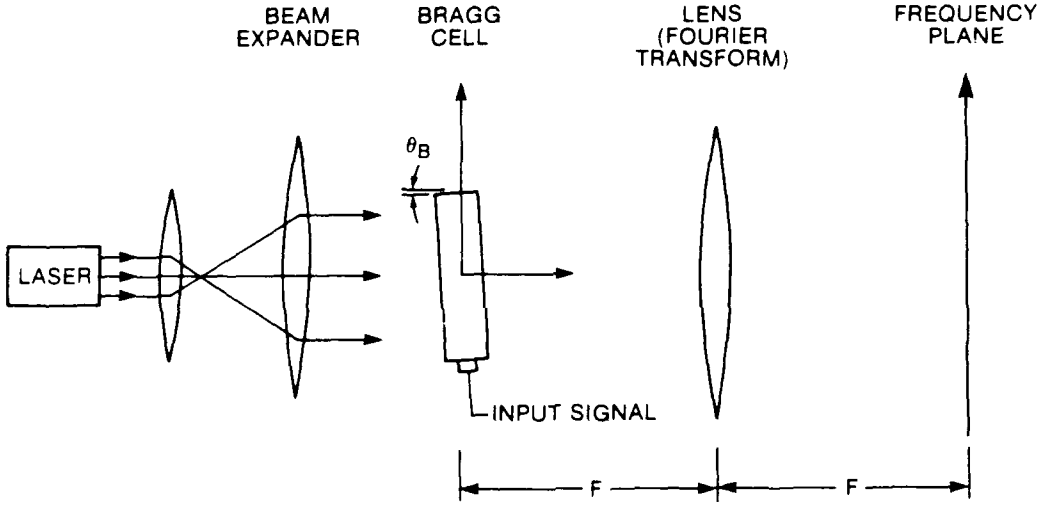

FIGURE 1: ACOUSTO-OPTIC SPECTRUM ANALYZER CONFIGURATION

The technological details and performance of the various components of this spectrum analyzer are beyond the scope of this report but are currently the object of active research. It should be noted that the input signal is usually mixed with a local oscillator signal to obtain a signal within the passband of the Bragg cell transducer.

Theoretical formulation and experimental results of the spectrum analysis performed by this type of configuration can be found in [2]. A mathematical model that is frequently used to describe the signal processing of this AOSA with an integrating photodetector array and the one that will be used throughout this report is represented by the following equation [3][4]:

$$X_{jk} = \int_{jI}^{(j+1)I} \int_{-\infty}^{\infty} H(f-f_k) \left| \int_{-\infty}^{\infty} \omega(z)u(t-z)\exp(-i2\pi fz)dz \right|^2 df\, dt \qquad (1)$$

where X_{jk} is the voltage produced at the output of the k^{th} detector for the j^{th} time frame. In this equation, $u(t)$ is the input signal, $\omega(z)$ is the window function determined by the Bragg cell and the shaping of the laser beam, f_k is the frequency associated with the k^{th} detector, $H(f)$ is a spectral weighting function that describes the spatial response of an individual detector element and I is the integration time of the detectors. This equation implies that the instantaneous light intensity distribution shining on the array of photodetectors is the magnitude squared Fourier transform of the part of the signals that are contained in the Bragg cell at that time windowed by the function $\omega(z)$. Each photodetector in the focal plane spatially integrates the light intensity distribution and converts it to currents which are integrated and sampled at periodic intervals.

Figure 2 illustrates the time variation of the light intensity distribution shining on the array of photodetectors as the pulse modulated carrier signal of frequency f_o propagates through the Bragg cell for the case where the pulse width (PW) is smaller than τ, which is the time duration needed for the acoustic wave to travel completely across the Bragg cell. In that Figure, the dotted line represents the Bragg cell and the solid line represents the envelope of the pulse modulated carrier as it propagates through the cell.

Figure 3 is the same as Figure 2 except that it illustrates the time variation of the light intensity distribution for the case where PW $>$ τ. We note that for that case, the narrowness of the light distribution is limited by the finite width of the Bragg cell.

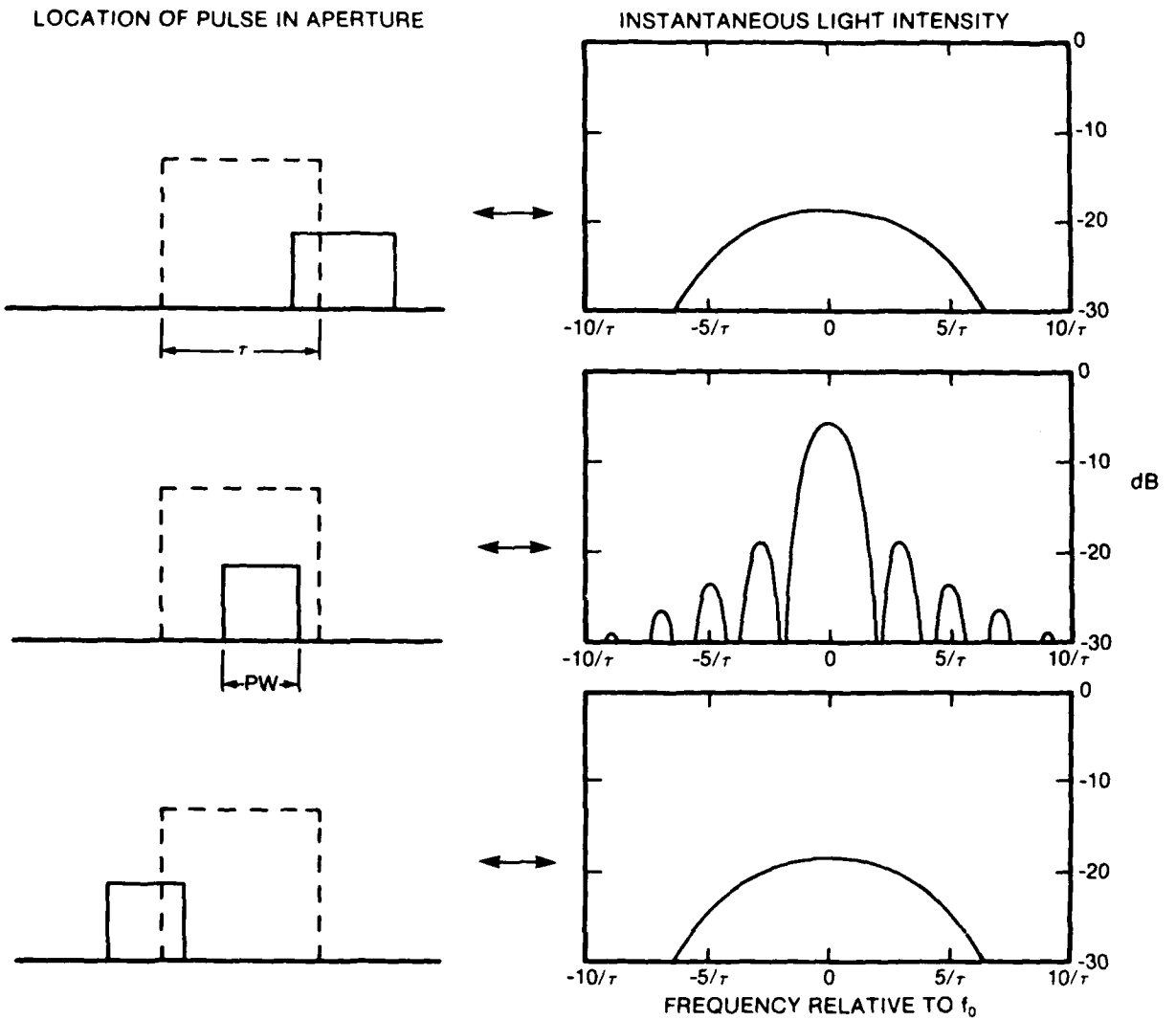

FIGURE 2: TYPICAL TIME VARIATION OF ILLUMINATION PATTERN (PW < τ)

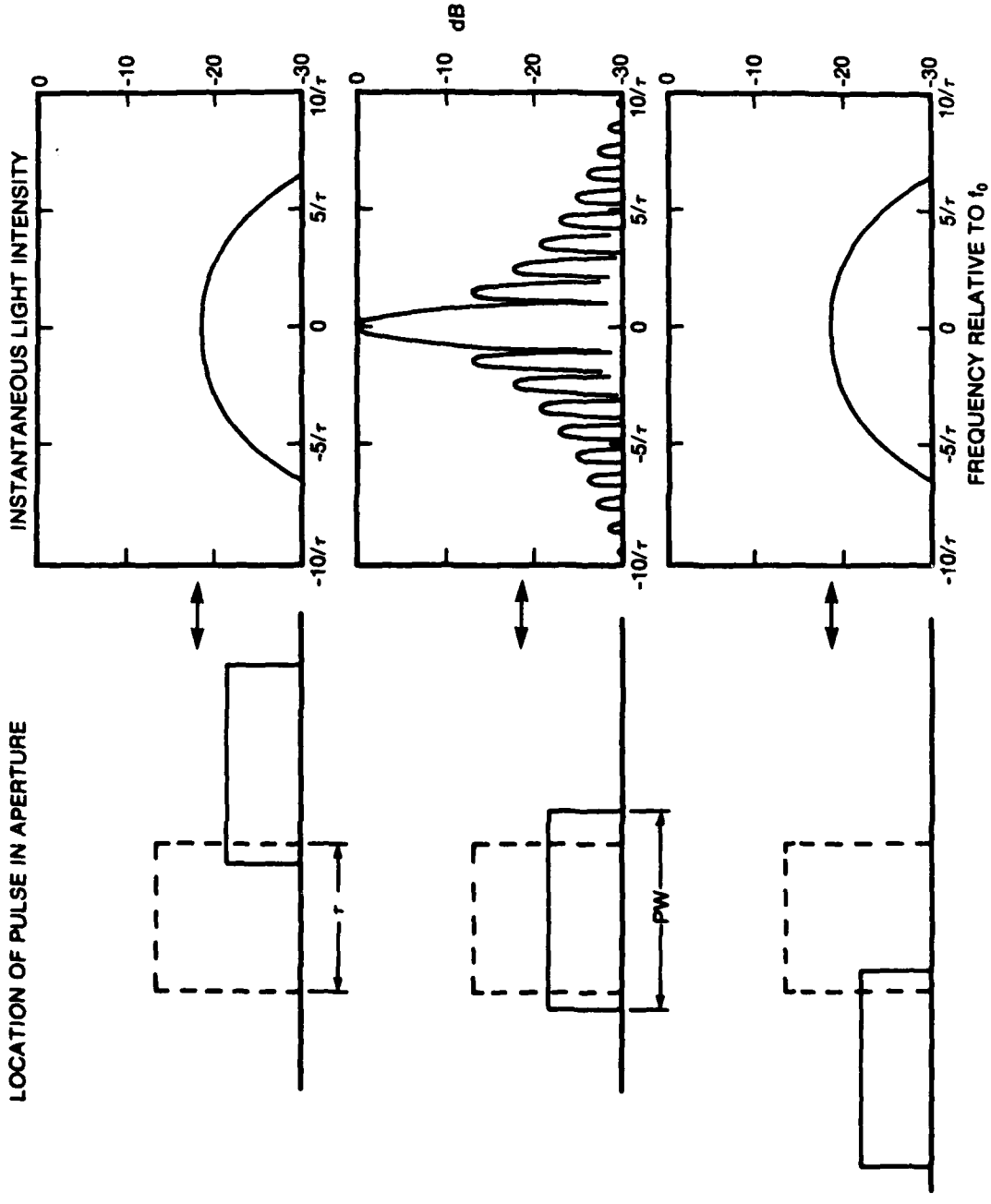

FIGURE 3: TYPICAL TIME VARIATION OF ILLUMINATION PATTERN (PW > τ)

In both Figures 2 and 3 we have represented the Bragg cell window, $\omega(z)$, as a rectangular window which means that the instantaneous light distribution is a squared Sinc function. This is the window that will be used in this report but in [5] we show how the signals can be calculated when we take into account the exponential losses of the Bragg cell and the Gaussian shaping of the laser beam.

In this report, it will be assumed that H(f) is a rectangular function of unit amplitude and width B Hz, symmetrical about f = 0. As it was mentioned before, H(f) is in fact a spatial weighting function describing the response of an individual photodetector, but there is a linear one-to-one correspondence between the spatial and spectral responses due to the fact that the angle of diffraction is proportional to the frequency of the input signal.

As an example of the types of signals that need to be processed, Figure 4 shows the output of the AOSA for a continuous wave (CW) signal of frequency f_o and when $\tau B = 3$ for the case where $\omega(z)$ is a rectangular function. Figure 5 shows the output when $\tau B = 6$ with the other parameters being the same as for Figure 4. Both of these figures show the output when f_o corresponds to one f_k as well as when f_o is exactly in the middle of two f_k's.

In this report we will assume that the input is a CW signal, but as discussed in [5] the analysis can easily be applied to pulse modulated signals by changing the constant τB. For example, if the pulse width is $\tau/5$, then considering the case for $\tau B/5$ where τB is the actual constant will give accurate results. For a certain range of pulse widths this will introduce errors but these will be ignored. The reader is referred to [5] for a more complete discussion of this matter.

2.2 Noise

Harms and Hummels [4] have done some numerical calculations on the probability density functions for the noise at the output of the AOSA assuming that Gaussian noise is present at the front end of the receiver. However, depending on the receiver, it is not clear whether this will be the dominant source of noise. It could be that the photodetectors are the dominant source of noise. In [6] we have measured the noise of an Avalanche Photodiode (APD) array and we have found that it can be well characterized by the Gaussian or Normal distribution. Other components such as logarithmic amplifiers and buffers will also introduce noise and the Central-Limit Theorem [7] tells us that the distributions of a large number of independent noise sources will tend toward the Normal or Gaussian probability distribution function (PDF). Hence, for the above reasons and for mathematical simplicity, we will assume in this report that the noise components of each photodetector can be modelled by independent Gaussian random variables with equal variance. In practice, the mean values of these random variables will not be zero but we have shown in [8] how we can correct for these offset errors. Therefore the noise model that will be used in this report represents each photodetector output as a signal component plus a zero-mean Gaussian random variable that is independent of the other random variables but that has the same variance as the other random variables.

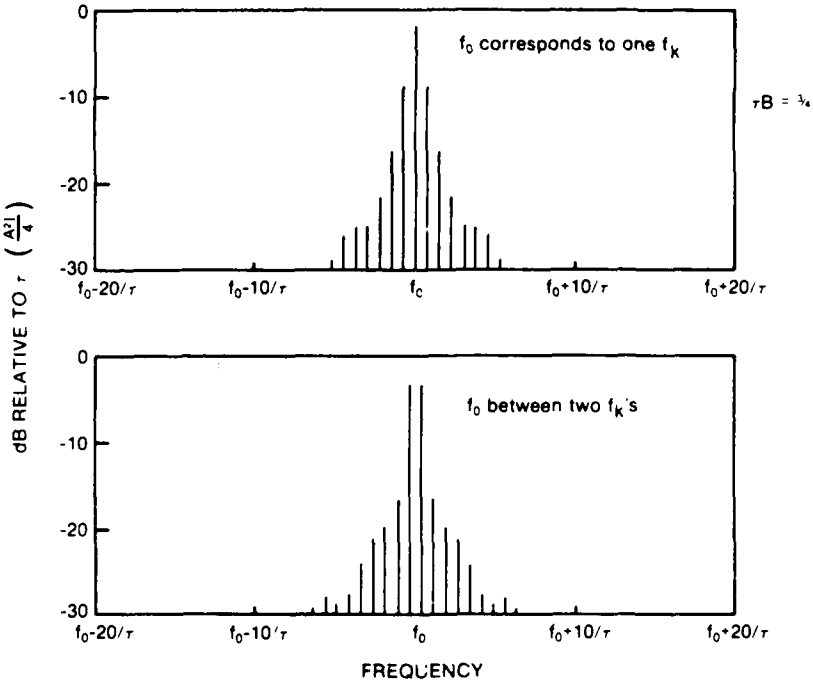

FIGURE 4: OUTPUT OF AOSA ($\omega(z)$ IS A RECTANGUALR FUNCTION, $\tau B = 3/4$)

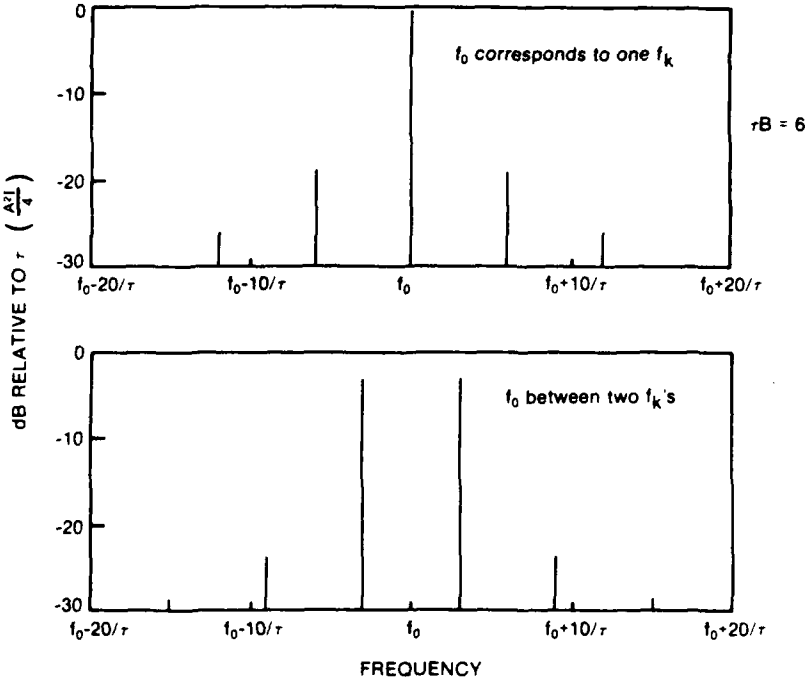

FIGURE 5: OUTPUT OF AOSA ($\omega(z)$ IS A RECTANGUALR FUNCTION, $\tau B = 6$)

3.0 CRAMER-RAO BOUND

Using the model described in the preceding section, we will, in this section, present the Cramér-Rao bound for the estimation of the carrier frequency f_o. To this end, we let $\bar{R} = (r_1, r_2, r_3, \ldots r_N)$ be the received vector where the r_i's are the pixel output values for a given integration time frame. We can write

$$r_i = m_i + n_i, \quad i = 1, 2, 3, \ldots, N \tag{2}$$

where the n_i's are independent, zero-mean, Gaussian random variables with variance σ^2, the m_i's are the signal components and N is the number of pixels in the photodetector array. It should be noted in relation to equation (1) that $m_i = x_{ji}$. This means that the conditional probability of the received vector $\bar{R}$ given that the carrier frequency of the input signal is f_o is:

$$P(\bar{R}|f_o) = \prod_{i=1}^{N} \frac{1}{\sqrt{2\pi}\,\sigma} \exp\left(\frac{-(r_i - m_i)^2}{2\sigma^2} \right) \tag{3}$$

where the m_i's are the signal components for frequency f_o. From [9] we have that an expression for the Cramér-Rao inequality is:

$$\mathrm{Var}\left[f_o^{e}(\bar{R}) - f_o \right] \geq \left(E\left(\left[\frac{\partial \ln P(\bar{R}|f_o)}{\partial f_o} \right]^2 \right) \right)^{-1} \tag{4}$$

where $f_o^{e}(\bar{R})$ is any unbiased estimator of f_o.

Taking the natural logarithm on both sides of equation (3) we get:

$$\ln\left(P(\bar{R}|f_o) \right) = -N \ln\left(\sqrt{2\pi}\,\sigma\right) - \sum_{i=1}^{N} \frac{(r_i - m_i)^2}{2\sigma^2} \tag{5}$$

Taking the partial derivative with respect to f_o we get:

$$\frac{\partial \ln P(\bar{R}|f_o)}{\partial f_o} = \frac{1}{\sigma^2} \sum_{i=1}^{N} (r_i - m_i)\, m_i' \tag{6}$$

where $m_i' = \frac{\partial m_i}{\partial f_o}$. Squaring both sides of equation (6) we get:

$$\left[\frac{\partial \ln P(\bar{R}|f_o)}{\partial f_o}\right]^2 = \frac{1}{\sigma^4}\left(\sum_{i=1}^{N}(r_i m_i' - m_i m_i')^2 + \sum_{\substack{i=1 \\ j\neq i}}^{N}\sum_{j=1}^{N}(r_i m_i' - m_i m_i')(r_j m_j' - m_j m_j')\right) \quad (7)$$

expanding the terms of equation (7) we obtain:

$$\left[\frac{\partial \ln P(\bar{R}|f_o)}{\partial f_o}\right]^2 = \frac{1}{\sigma^4}\sum_{i=1}^{N}(r_i^2(m_i')^2 + m_i^2(m_i')^2 - 2 r_i m_i(m_i')^2 + \frac{1}{\sigma^4}\sum_{\substack{i=1 \\ j\neq i}}^{N}\sum_{j=1}^{N}$$

$$(r_i m_i' r_j m_j' - r_i m_i' m_j m_j' - m_i m_i' r_j m_j' + m_i m_i' m_j m_j') \quad (8)$$

Now $E(r_i) = m_i$ and $E(r_j) = m_j$ and since r_i, r_j are independent provided that $i\neq j$, then $E(r_i r_j) = E(r_i)E(r_j) = m_i m_j$. Also, it is easy to show that $E(r_i^2) = \sigma^2 + m_i^2$. Using these identities and simplifying we get that:

$$E\left(\left[\frac{\partial \ln P(\bar{R}|f_o)}{\partial f_o}\right]^2\right) = \sum_{i=1}^{N}\frac{(m_i')^2}{\sigma^2} \quad (9)$$

Combining equations (4) and (9) we get that the Cramér-Rao inequality for this problem is:

$$\mathrm{Var}\left[f_o^e(\bar{R}) - f_o\right] \geq \frac{\sigma^2}{\sum_{i=1}^{N}(m_i')^2} \quad (10)$$

We have shown in [5] that for a sinusoidal input, $u(t) = A \cos(2\pi f_o t + \phi)$,

$$m_k = \frac{A^2 I}{4} O(f_k - f_o) \tag{11}$$

where $O(f)$ is the convolution between the functions G and H,

$$O(f) = \int_{-\infty}^{\infty} H(f - f') G(f') df' \tag{12}$$

where $G(f)$ is the magnitude squared of the Fourier transformed window function,

$$G(f) = \left| \int_{-\infty}^{\infty} w(z) \exp(-i2\pi fz) dz \right|^2 \tag{13}$$

As it was mentioned in the previous section, in this report we will use an $H(f)$ which is a rectangular function of unit amplitude and width B Hz symmetrical about f=0 and a $w(z)$ which is a rectangular window whose duration is the time taken for the acoustic wave to travel across the Bragg cell and we will call this time τ. For this case we have that

$$G(f) = \tau^2 \frac{\sin^2(2\pi f\tau/2)}{(2\pi f\tau/2)^2} \tag{14}$$

There is no closed form solution to equation (12) but using numerical integration and differentiation programs we can calculate the variance of the efficient estimator, Var_{eff} which is the equality case of equation (10). We are interested in knowing how the efficient estimator varies as a function of the frequency f_o. We found that for a given τB the variance of the efficient estimator was periodic with a period of B Hz provided that the frequency of the input signal did not correspond to a frequency near the edge of the array.

We are also interested in knowing how the efficient estimator varies as a function of the constant τB. This constant is a basic design parameter and does not change for a given system. It is a measure of the coarseness of the spatial sampling from the photodetectors as can be seen by comparing Figure 4 and Figure 5.

It should be noted that the number of pixel values that we include in our calculations does not have to be N, which is the number of photodetectors in the array. The reason for this is that, for many of those pixels, the values of the m_i's are relatively small. Hence, we have included in our calculations as many pixels as was required but not more since this would uselessly increase the number of computations and we will call this number n. Using 55 pixels, we find that for $\tau B = \frac{1}{4}$ the variance of the efficient estimator is quite constant as we vary the input frequency and

$$\sqrt{Var_{eff}} = 1.27 \times \frac{4\sigma}{\tau^2 A^2 I}$$

whereas for $\tau B = \frac{1}{2}$ we find that it is also fairly constant except that in this case

$$\sqrt{Var_{eff}} = 0.98 \times \frac{4\sigma}{\tau^2 A^2 I}$$

where $\sqrt{Var_{eff}}$ is the root mean squared (RMS) error for the efficient estimator which we will henceforth call RMS_{eff}. Letting

$$K = \frac{A^2 I \tau}{4\sigma}$$

Figures 6 to 10 show RMS_{eff} x($K\tau$) as a function of the frequency offset x(τ), which is the difference between the input frequency f_o and the corresponding frequency of the closest pixel. When f_o exactly corresponds to one of the f_k's then this frequency offset is zero. In these Figures we have only plotted RMS_{eff} over one period because as was mentioned earlier, RMS_{eff} as a function of frequency is periodic with period B Hz.

It should be noted that the constant K is a figure of merit for the detection probability. This means that the detection probability for a given signal increases as the value of K increases, everything else remaining the same. It is important to note that the integration time of the photodetectors (I) and the Bragg cell aperture time (τ) are equally strong contributors to the increase of K. However, in the case of pulse modulated signals, this latter contribution will only be efficient if the signal is present during the whole time that the photodetectors are integrating. For example, if we have a 50 ηsec pulse that enters a Bragg cell with a 1 μsec aperture time and the integration time of the photodetectors is 10 μsec, then increasing the integration time of the photodetectors beyond 10 μsec will not increase the detection probability for that signal.

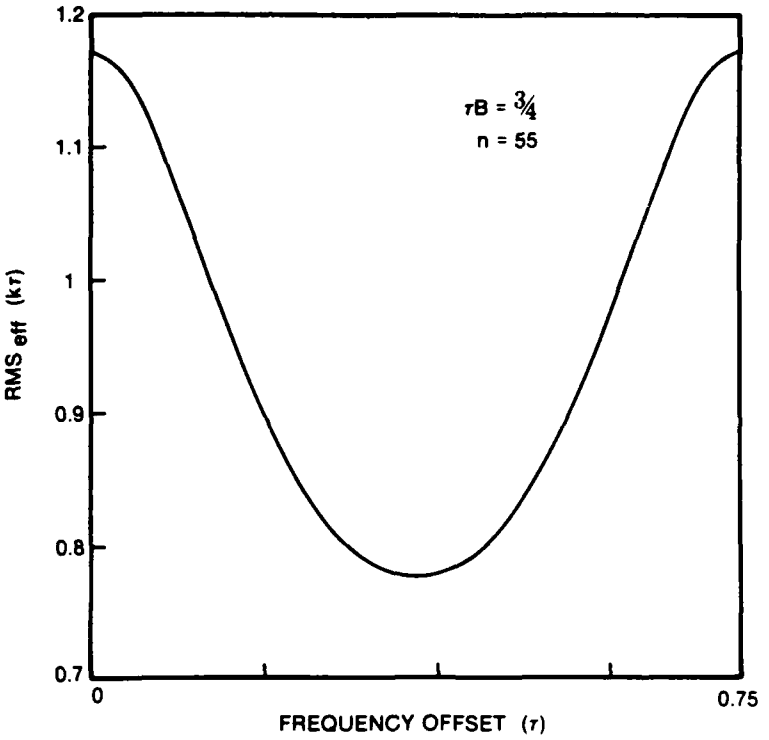

FIGURE 6: RMS_{eff} WHEN $\tau B = \frac{3}{4}$

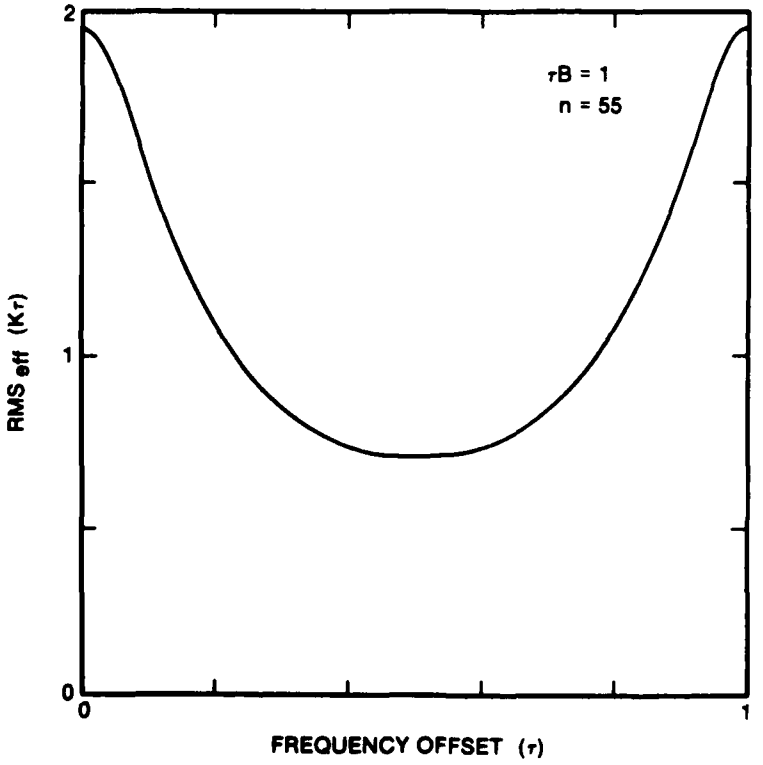

FIGURE 7: RMS_{eff} WHEN $\tau B = 1$

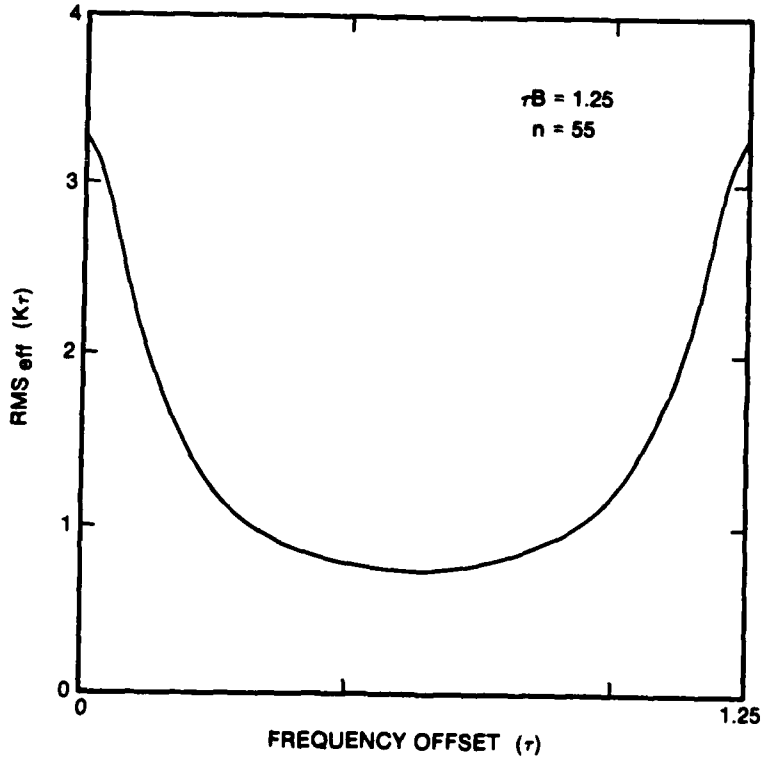

FIGURE 8: RMS_{eff} WHEN $\tau B = 1.25$

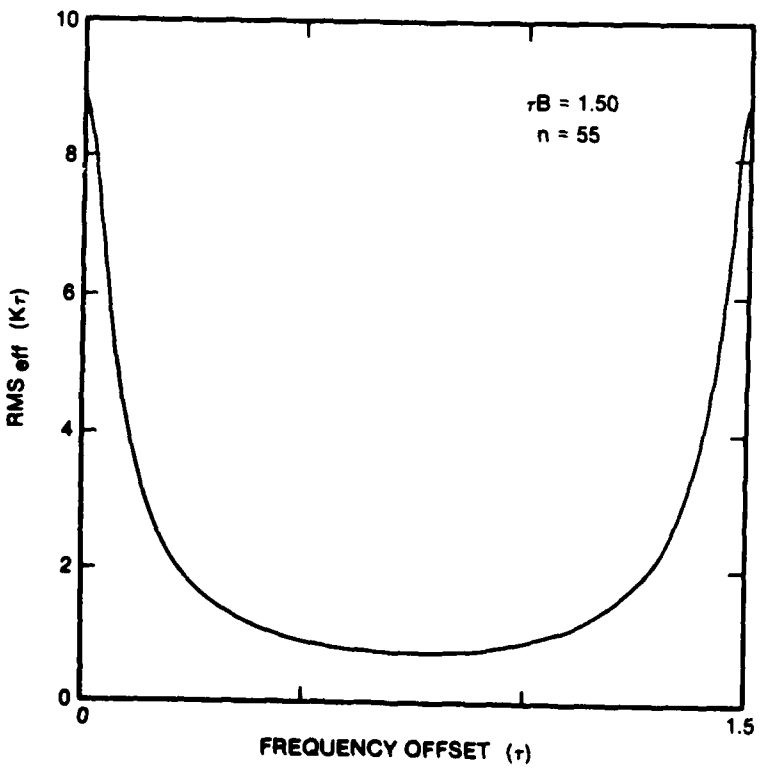

FIGURE 9: RMS_{eff} WHEN $\tau B = 1.5$

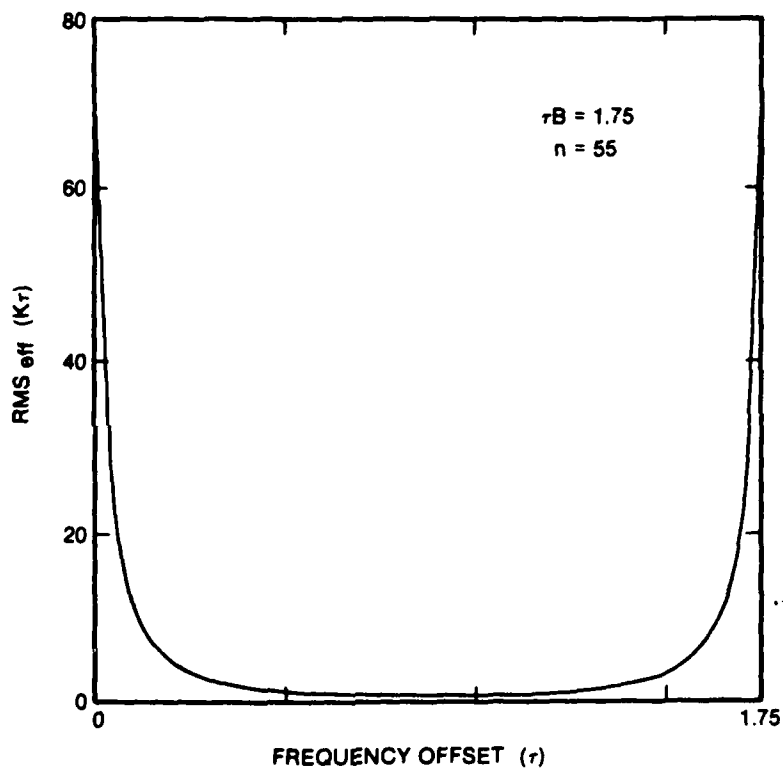

FIGURE 10: RMS_{eff} WHEN $\tau B = 1.75$

Since the input frequency f_o could be any frequency, it is interesting to know what is the average RMS_{eff}. This can be done by averaging curves such as those in Figures 6 to 10. This has been done for several values of the constant τB and the result is as shown in Figure 11. We see from this curve that the average RMS_{eff} is relatively small when τB is between 0.25 and 1.25 but it increases exponentially as τB is closer to 2. Figure 12 demonstrates this more clearly as it shows the average RMS_{eff} for higher values of τB. It should be noted on this Figure that the average RMS_{eff} for values of the constant τB in the proximity of 2, 3 and 4 are actually off scale. The actual value of the average RMS_{eff} for $\tau B = 3$ is $241/K\tau$ whereas for $\tau B = 2$ and 4 it is several orders of magnitude higher.

Since Figure 12 gives us a lower bound for any unbiased estimator, it is clear that any such estimator would have a very undesirable performance for τB greater than 1.75. In fact, we could even doubt that an unbiased estimator even exists for some of these values of τB.

4.0 PEAK DETECTION

In the previous section, we have presented the Cramér-Rao lower bound on the variance of any unbiased estimator for this problem. We have found that this bound increases exponentially as the value of the constant τB increases higher than 1.75 and that it even peaks at extremely high values in the vicinity of certain values of τB. This means that any unbiased estimator for this problem would have a poor performance for values of τB greater than 1.75 and, in fact, it is probably impossible to find an unbiased estimator for this problem for some of these values of τB.

In this section, we present the performance of the peak detector estimator for this problem. That is, we present the performance of the algorithm that assumes that the frequency of the input signal is the frequency that corresponds to the highest pixel value. This is a very natural and simple algorithm to use for this problem and it does not depend on the shape or the width of the light intensity distribution. This latter characteristic is especially attractive in the RESM context where the receiver would have to detect signals with many different pulse widths, some being very small and others very large.

To this end, let us first assume that $X_1, X_2, X_3, \ldots, X_N$ are N independent Gaussian random variables with equal variance σ^2 for which the means are $\bar{X}_1, \bar{X}_2, \bar{X}_3, \ldots, \bar{X}_N$ respectively. This means that the probability density functions for these random variables are

$$f(x_i) = \frac{1}{\sigma\sqrt{2\pi}} \exp\left(\frac{-(x_i - \bar{X}_i)^2}{2\sigma^2}\right), \quad i = 1, 2, 3, \ldots, N \tag{15}$$

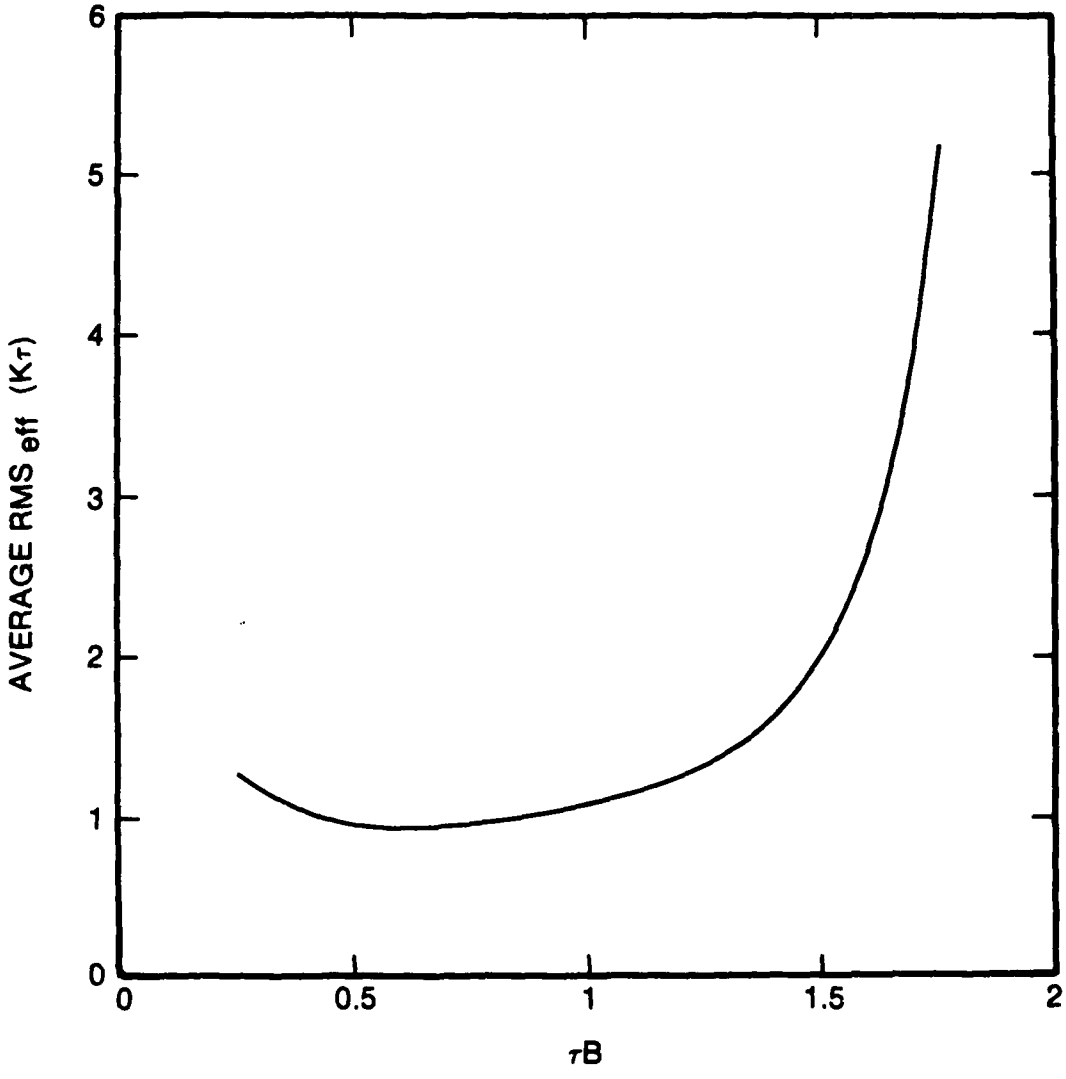

FIGURE 11: AVERAGE RMS ERROR OF THE EFFICIENT ESTIMATOR

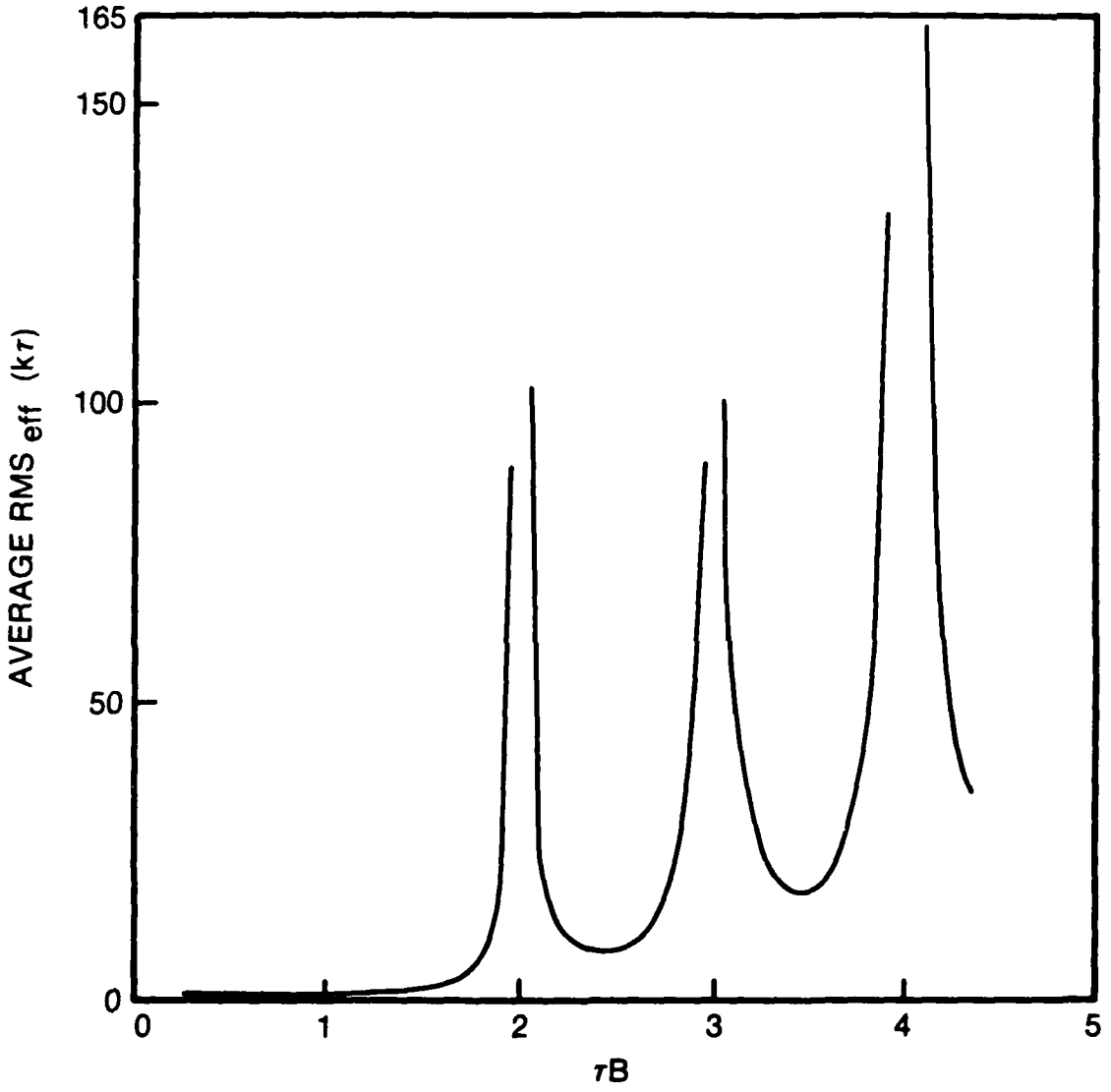

FIGURE 12: AVERAGE RMS ERROR OF THE EFFICIENT ESTIMATOR

and since these random variables are independent we can write their joint density function as

$$f(x_1, x_2, x_3, \ldots, x_N) = \frac{1}{(\sigma\sqrt{2\pi})^N} \prod_{i=1}^{N} \exp\left(\frac{-(x_i - \bar{X}_i)^2}{2\sigma^2}\right) \tag{16}$$

If we define ψ_j as the probability that the random variable X_j is higher than all the others, then it can be evaluated by the following N integrals

$$\psi_j = \int_{-\infty}^{\infty} \overbrace{\int_{-\infty}^{x_j} \int_{-\infty}^{x_j} \int_{-\infty}^{x_j} \cdots \int_{-\infty}^{x_j}}^{(N-1)\text{ times}} f(x_1, x_2, x_3, \ldots, x_N)\left(\prod_{\substack{i=1 \\ i\neq j}}^{N} dx_i\right)dx_j \tag{17}$$

which, after a change of variables, can be rewritten

$$\psi_j = \int_{-\infty}^{\infty} \frac{1}{\sigma\sqrt{2\pi}} \exp\left(\frac{-(x_j - \bar{X}_j)^2}{2\sigma^2}\right) \prod_{\substack{i=1 \\ i\neq j}}^{N} \left(\tfrac{1}{2}\left[1 + \operatorname{derf}\left(\frac{x_j - \bar{X}_i}{\sqrt{2}\ \sigma}\right)\right]\right) dx_j \tag{18}$$

where

$$\operatorname{derf}(y) = \frac{2}{\sqrt{\pi}} \int_{0}^{y} \exp(-t^2)dt, \text{ for y positive}$$

$$= \frac{-2}{\sqrt{\pi}} \int_{0}^{-y} \exp(-t^2)dt, \text{ for y negative} \tag{19}$$

Using equation (18) we get the RMS error for the peak estimator

$$RMS_{pk} = \sqrt{\sum_{j=1}^{N} (f_j - f_o)^2 \psi_j} \tag{20}$$

and also the mean error for this estimator

$$Mean_{pk} = \sum_{j=1}^{N} (f_j - f_o) \psi_j \tag{21}$$

Figures 13 and 14 show RMS_{pk} and $Mean_{pk}$ respectively for the case of $\tau B = 0.5$, $n = 15$, and $K = A^2 I\tau/4\sigma = 10$.

Figures 15 and 16 show RMS_{pk} and $Mean_{pk}$ respectively for the same case except for $K = 20$. Again in these figures we have plotted only one period of these functions since they are periodic with period B Hz.

We see from Figures 14 and 16 that the peak estimator is actually a biased estimator for a given input frequency. However, it has the desired characteristic of a zero average bias over many different input frequencies. This can be seen by the symmetry of Figures 14 and 16.

As we have done with the Cramér-Rao bound, we can obtain the average RMS_{pk} by averaging curves such as those of Figures 13 and 15. This has been done for several values of the constant τB for a given K. Figure 17 shows the resulting family of curves for several values of K. These curves have all been obtained by assuming 15 photodetectors in our calculations (i.e. n=15) so that we could compare the performance from a common basis. It should be noted that, for any given value of K, there is a value of τB which is really the smallest that would be used in practice. This is because the signal is so buried in the noise that the corresponding false alarm rate would be exceedingly high. We have not plotted points beyond that point on Figure 17. We see from that Figure that the smallest useful τB increases as we decrease the value of K. We also see from Figure 17 that for any given value of K, there is an optimum τB which gives the smallest RMS error. As in the case of the smallest useful τB, we see that this optimum τB increases as the value of K decreases.

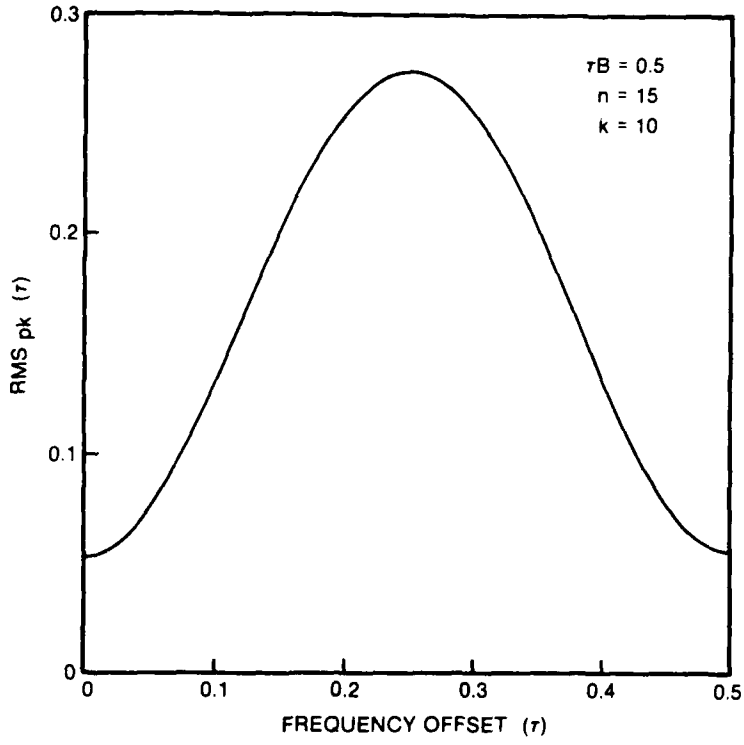

FIGURE 13: RMS ERROR FOR PEAK ESTIMATOR FOR $\tau B = 0.5$, $n = 15$, $K = 10$

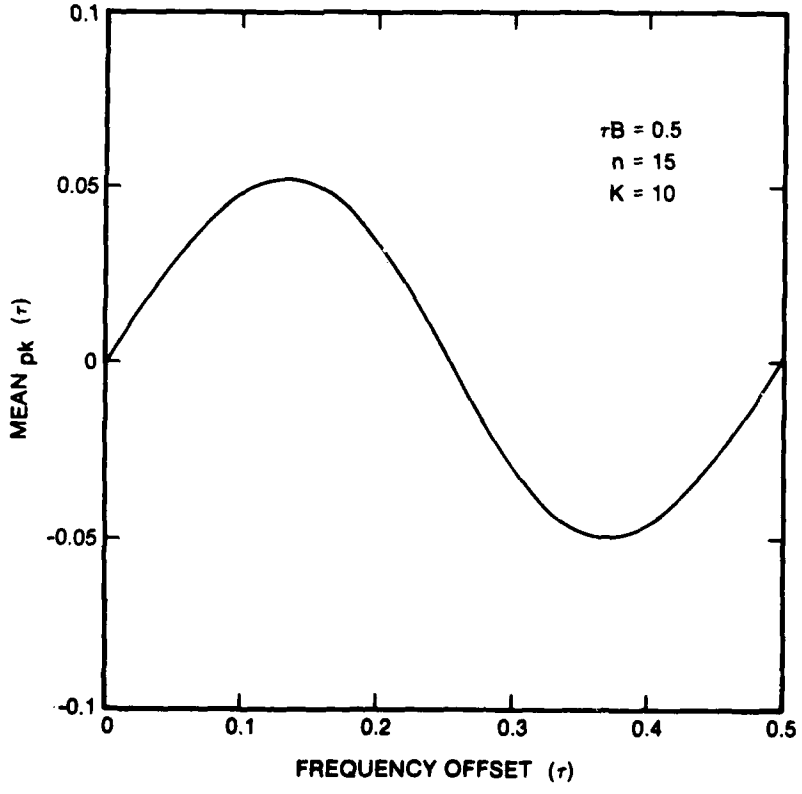

FIGURE 14: MEAN ERROR FOR PEAK ESTIMATOR FOR $\tau B = 0.5$, $n = 15$, $K = 10$

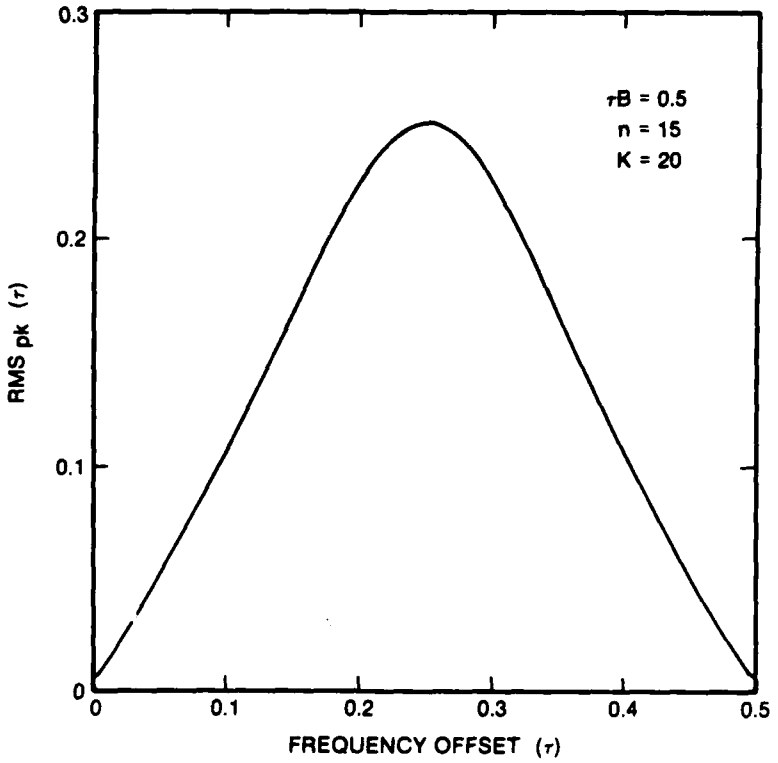

FIGURE 15: RMS ERROR FOR PEAK ESTIMATOR FOR τB = 0.5, n = 15, K = 20

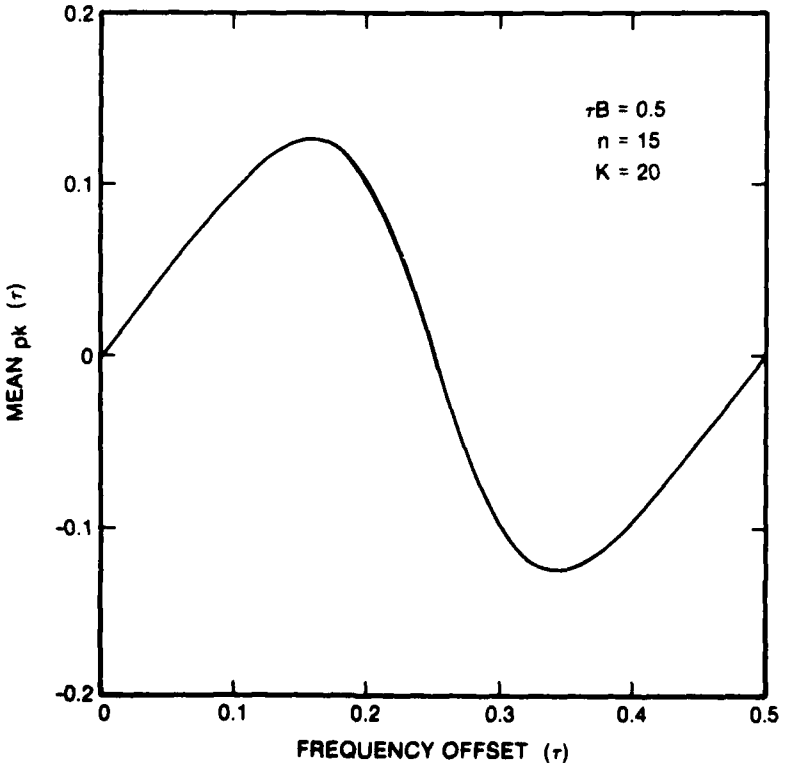

FIGURE 16: MEAN ERROR FOR PEAK ESTIMATOR FOR τB = 0.5, n = 15, K = 20

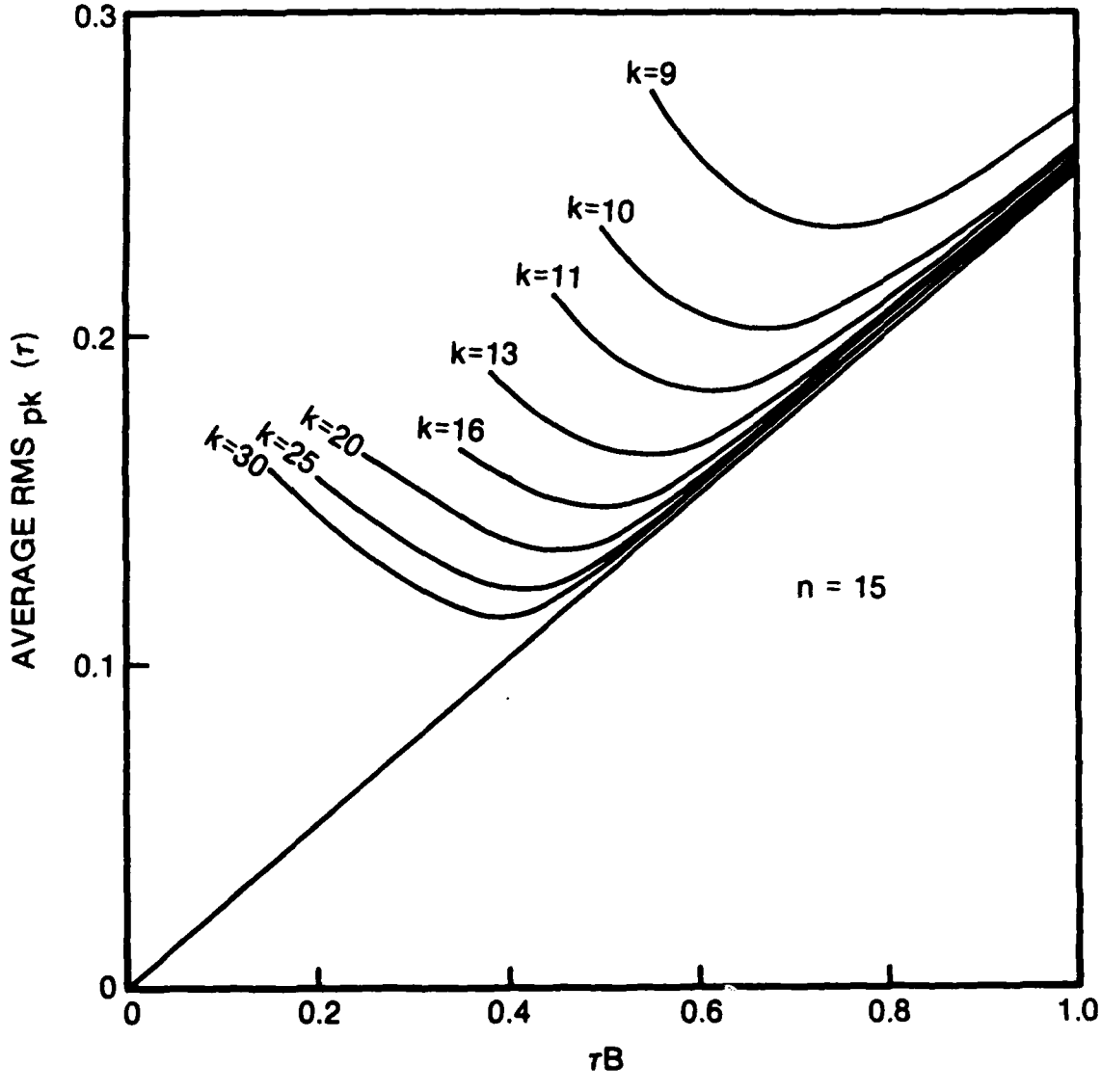

FIGURE 17: AVERAGE RMS ERROR OF THE PEAK ESTIMATOR

Finally, we note from Figure 17 that, for any value of K, the average RMS error for the peak estimator asymptotically tends towards a straight line as we increase the value of τB. So that we can see this better, we have plotted a straight line on Figure 17 that has a slope of $0.25/\tau$ and that passes through the origin.

This behaviour is to be expected and to see why let us consider the case of no noise or infinite signal to noise ratio. Figures 18 and 19 show the RMS error and the mean error (or the bias) of the peak detector estimator for this latter case. It is easy to see that the average RMS error in that case is B/4 and hence if $\tau B = a$, then the average RMS error will be $B/4 = a/4\tau$ which is in agreement with Figure 17.

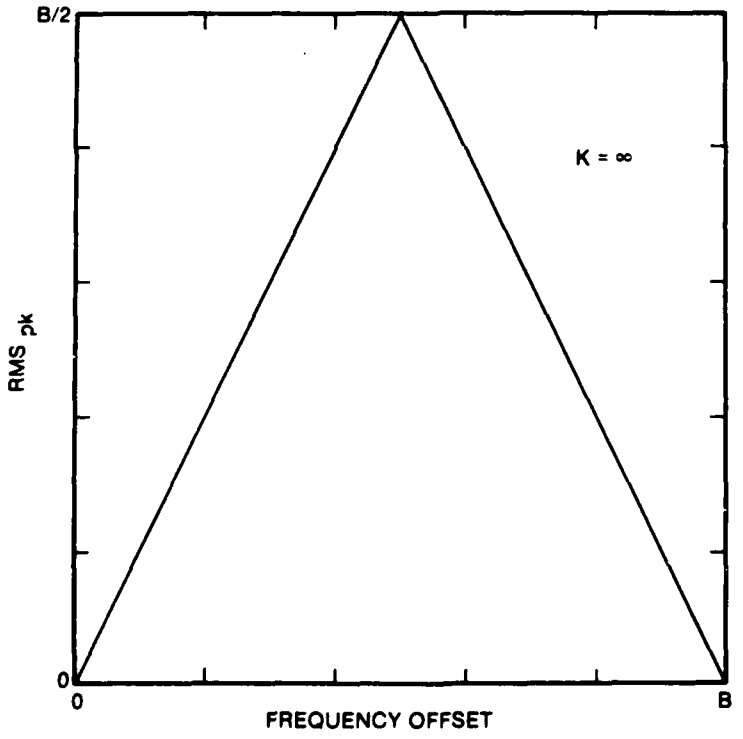

FIGURE 18: RMS ERROR OF PEAK ESTIMATOR WHEN K = ∞

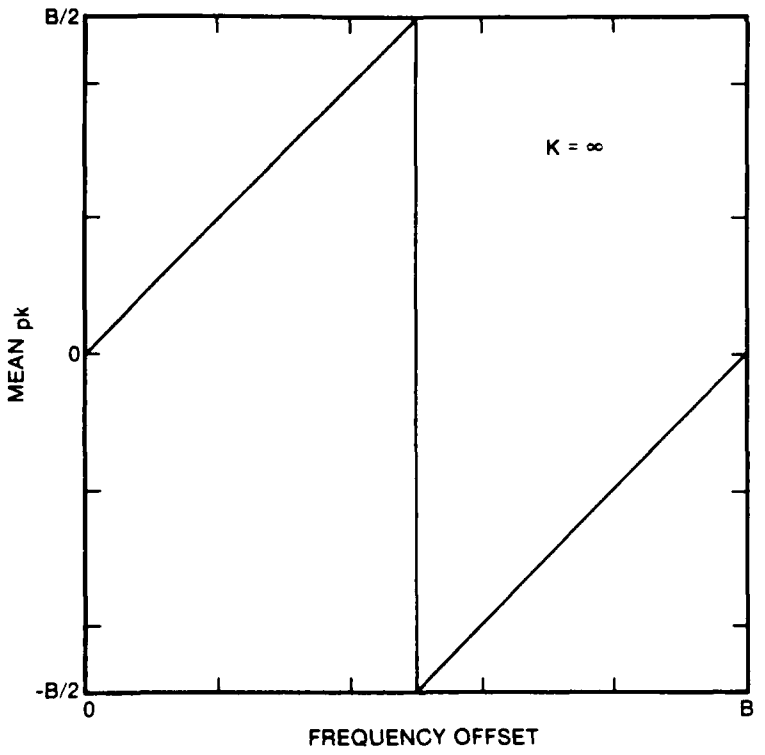

FIGURE 19: MEAN ERROR (BIAS) OF PEAK ESTIMATOR WHEN K = ∞

5.0 SIDELOBE REJECTION

In the previous section, we have analyzed the performance of the peak detector estimator as it is used to estimate the frequency of a radar signal. We have seen that this estimator, although being a biased estimator, is fairly well behaved and gives reasonably good performance aside from being simple and easy to implement. However, in the implementation of this algorithm, if we say that we have detected a peak whenever we have a situation where a pixel is higher than the two adjacent pixels on either side of it, then there may be cases where this algorithm will detect multiple frequencies when there is in reality only one signal present in the receiver of our AOSA. This situation occurs when the input signal has a very narrow pulse width (PW) in relation to τ and 1/B. For example, if we have an AOSA with a 500 MHz bandwidth, 125 photodetectors (hence, B = 4 MHz) and a Bragg cell aperture of 1 μsec (i.e. τ = 1 μsec), then the integrated photodetector outputs for a pulse modulated signal of 62.5 nsec (assuming I ≈ 1 μsec) would be as shown in Figure 20. As we can see from this Figure, the sidelobes of the signal give us a number of local peaks and it would be a serious mistake for an RESM receiver to report that there are multiple signals present simultaneously when in reality there is only one. It should be noted, however, that the extent to which this will be a problem will depend on the energy of the pulse that enters the AOSA front end and on the dynamic range and sensitivity of the AOSA. Since the AOSA

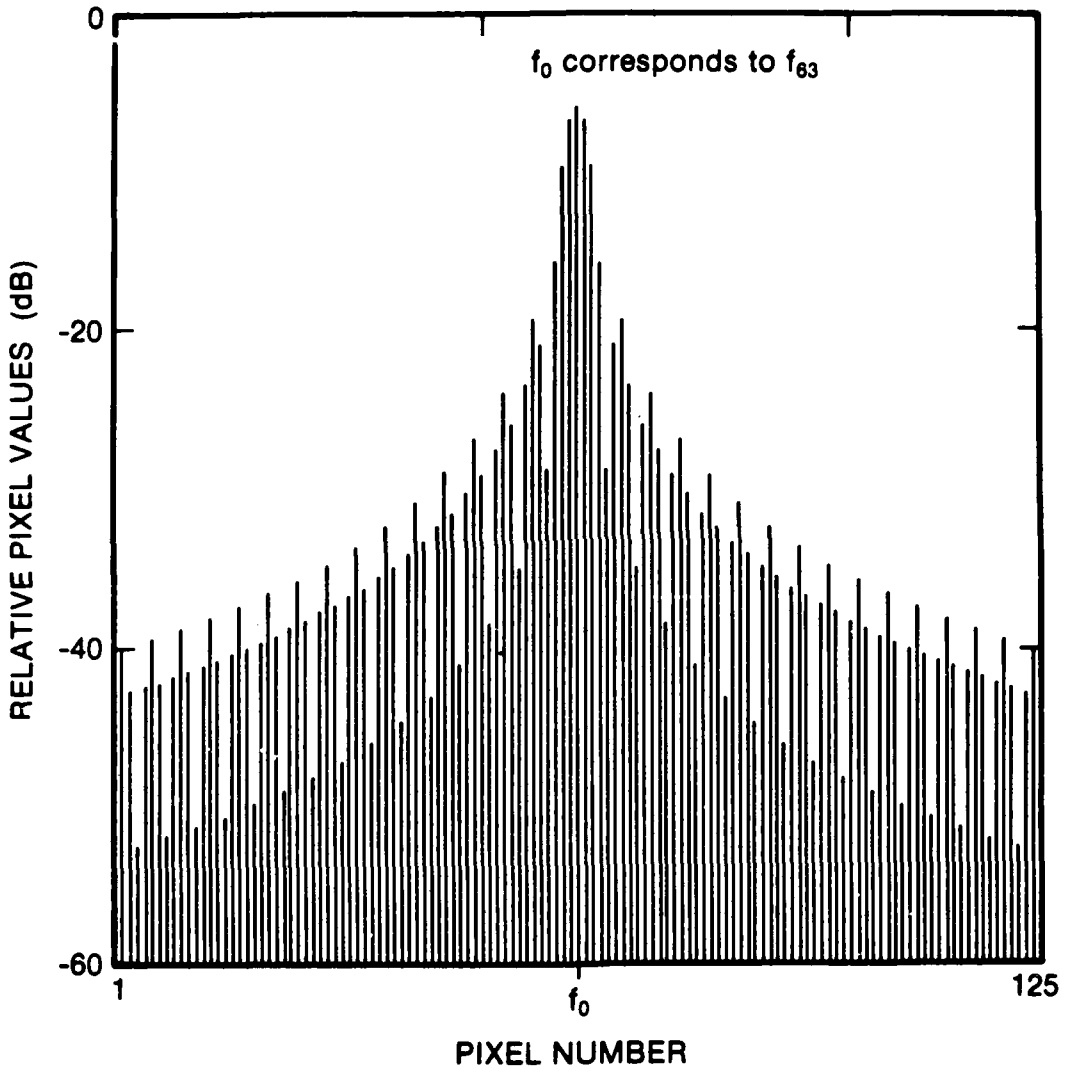

FIGURE 20: EXAMPLE OF AOSA OUTPUTS FOR A NARROW PULSE

basically measures the energy of the input signal in the respective frequency bins (which are determined by the photodetector widths), either the AOSA will have to have the required sensitivity and dynamic range or the pulse will have to enter the receiver with significant power for the sidelobes to show as they do in Figure 20. But nonetheless, since this would be a very undesirable situation, then something should be done so that the signal is not interpretted as a multiplicity of signals. This means that we must find an algorithm that rejects the sidelobes of a narrow pulse and does not erroneously assume that they are multiple signals.

The solution that we propose for this problem is that we should define a local peak by considering more pixels than simply the two adjacent pixels on both sides of the pixel under consideration. This algorithm is explained by the conceptual block diagram of Figure 21. We see in that Figure that we consider a window of L pixels (where L is an odd number) to determine whether a signal is present or not. That is, the pixel in register L/2 + 1 must be higher or equal to the L/2 pixels on each side of it in order for us to assume that there is a signal present which has a carrier frequency equal to the frequency associated with the L/2 + 1 register. We assume in that Figure that the data is coming in serially although we have shown in [8] how we could easily handle data that is parallel.

This algorithm is easy to implement even at high speeds. It works equally well on linear or logarithmic data and it adapts well to different signals. It should be noted that, since the condition applied is that $B \geq A$, there could be instances where we report two signals being present. This would happen, for example, if the input signal frequency is exactly between two f_k's as in Figures 4 and 5. This would be a very unlikely situation in a practical system especially in the presence of noise but it could happen and it should be taken into consideration in further stages of processing.

It should be pointed out that this algorithm will limit our ability to resolve two signals closely spaced in frequency. Therefore, the choice of L should be made judiciously according to the knowledge that we have about the types of signals that we could be processing. Making L equal to the number of photodetectors in our array, for example, would completely preclude us from detecting more that one signal per integration frame, a situation which is completely unacceptable. Or making L = 3, as another example, would cause us to report multiple signals for the situation of Figure 20, a situation which is equally unacceptable. However, relatively small filter lengths are required for this algorithm. A filter length of L = 9, for example, would be adequate for the situation of Figure 20.

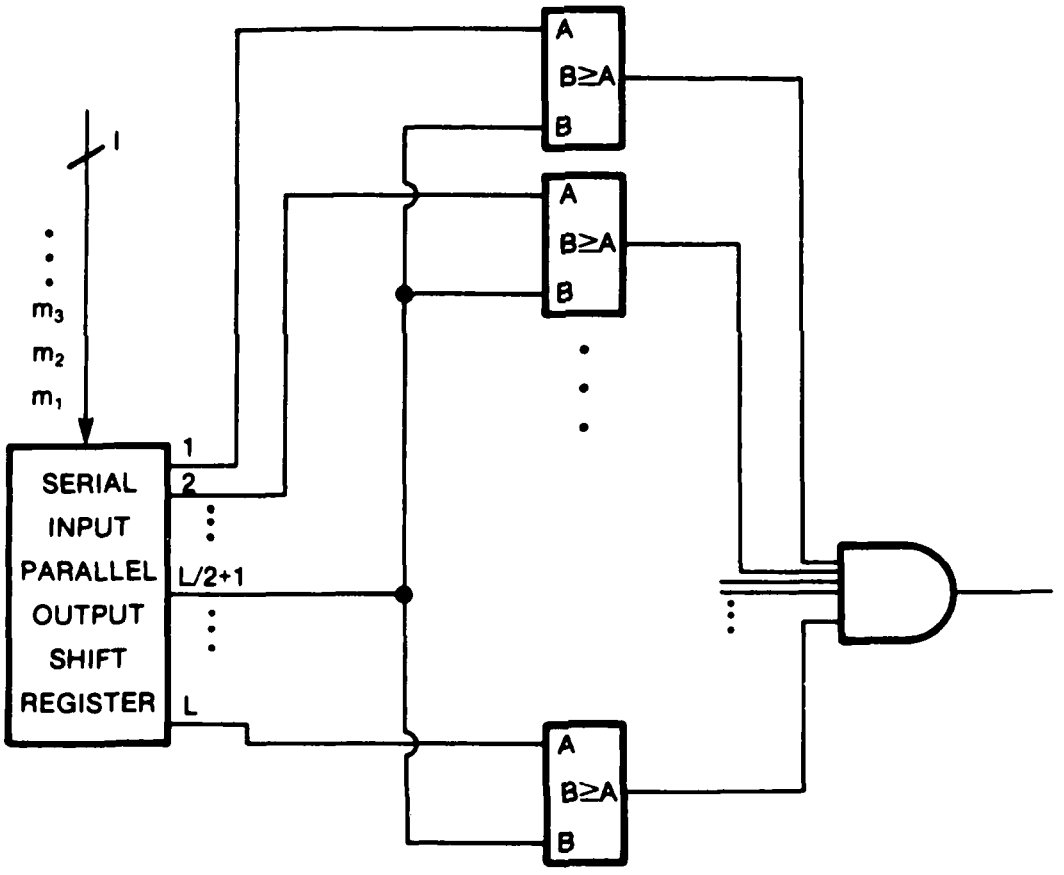

FIGURE 21: SIDELOBE REJECTION ALGORITHM

6.0 CONCLUDING REMARKS

We have presented a model for the signals of an AOSA and we have used it to study the problem of estimating the carrier frequency of radar signals. To this end, we have calculated the Cramér-Rao bound which indicated that any unbiased estimator for this problem would have a poor performance for τB greater than 1.75. In our quest for a good biased estimator, we have calculated the performance of the peak detector estimator which, although being a biased estimator, actually has the desired characteristic of having a zero average bias over many different input frequencies. Finally, we have also presented an algorithm to reject the sidelobes, a problem which may arise in certain cases where we apply the peak detector estimator.

7.0 REFERENCES

[1] Davies, C.L. and Hollands, B.A., "Automatic Processing for ESM", IEE Proceedings Part F, Vol. 129, Pt F, No. 3, pp. 164-171, June 1982.

[2] Lee, Jim P.Y., "Acousto-Optic Spectrum Analysis of Radar Signals Using an Integrating Photodetector Array", Applied Optics, Vol. 20, No. 4, pp. 595-600, February 15, 1981.

[3] Kellman, Peter, et al, "Integrating Acousto-Optic Channelized Receivers", Proceedings of the IEEE, Vol. 69, No. 1, pp. 93-100, January 1981.

[4] Harms, B.K. and Hummels, D.R., "Analysis of Detection Probability for the Acousto-Optic Receiver", IEEE Transactions on Aerospace and Electronic Systems, Vol. AES-22, No. 4, pp. 326-339, July 1986.

[5] Farley, Guy, "Discussion on the Modelling and Processing of Signals from an Acousto-Optic Spectrum Analyzer" (U), Technical Note, DREO TN 87-13, June 1987. UNCLASSIFIED

[6] Farley, Guy and Hage, M., "Dark Noise Characterization of a 25-Element Avalanche Photodiode Array" (U), Technical Memorandum, DREO TM 86-29, November 1986.

[7] Papoulis, Athanasios, "Probability Random variables and Stochastic Processes", pp. 266, McGraw-Hill, 1965.

[8] Farley, G. and Inkol, R., "Post-Processor Design Concepts Applicable to an Acousto-Optic Spectrum Analyzer" (U), Technical Note, DREO TN 87-2, January 1987. UNCLASSIFIED

[9] Van Trees, Harry L., "Detection, Estimation and Modulation Theory, Part I", pp. 66, New York, Wiley, 1968.

SECURITY CLASSIFICATION OF FORM
(highest classification of Title, Abstract, Keywords)

DOCUMENT CONTROL DATA

(Security classification of title, body of abstract and indexing annotation must be entered when the overall document is classified)

1. ORIGINATOR (the name and address of the organization preparing the document. Organizations for whom the document was prepared, e.g. Establishment sponsoring a contractor's report, or tasking agency, are entered in section 8.)

DEPARTMENT OF NATIONAL DEFENCE
DEFENCE RESEARCH ESTABLISHMENT OTTAWA
SHIRLEY BAY, OTTAWA, ONTARIO K1A 0Z4 CANADA

2. SECURITY CLASSIFICATION (overall security classification of the document including special warning terms if applicable)

UNCLASSIFIED

3. TITLE (the complete document title as indicated on the title page. Its classification should be indicated by the appropriate abbreviation (S,C,R or U) in parentheses after the title.)

FREQUENCY ESTIMATION OF RADAR SIGNALS USING AN ACOUSTO-OPTIC SPECTRUM ANALYSER AS AN RESM RECEIVER (U)

4. AUTHORS (Last name, first name, middle initial. If military, show rank, e.g. Doe, Maj. John E.)

FARLEY, GUY J.

5. DATE OF PUBLICATION (month and year of publication of document)	6a. NO OF PAGES (total containing information. Include Annexes, Appendices, etc.)	6b. NO. OF REFS (total cited in document)
JUNE 1988	34	9

6. DESCRIPTIVE NOTES (the category of the document, e.g. technical report, technical note or memorandum. If appropriate, enter the type of report, e.g. interim, progress, summary, annual or final. Give the inclusive dates when a specific reporting period is covered.)

DREO TECHNICAL NOTE

8. SPONSORING ACTIVITY (the name of the department project office or laboratory sponsoring the research and development. Include the address.)

9a. PROJECT OR GRANT NO (if appropriate, the applicable research and development project or grant number under which the document was written. Please specify whether project or grant)	9b. CONTRACT NO (if appropriate, the applicable number under which the document was written)
011LB11	

10a. ORIGINATOR'S DOCUMENT NUMBER (the official document number by which the document is identified by the originating activity. This number must be unique to this document.)	10b. OTHER DOCUMENT NOS. (Any other numbers which may be assigned this document either by the originator or by the sponsor)

11. DOCUMENT AVAILABILITY (any limitations on further dissemination of the document, other than those imposed by security classification)

(X) Unlimited distribution
( ) Distribution limited to defence departments and defence contractors; further distribution only as approved
( ) Distribution limited to defence departments and Canadian defence contractors; further distribution only as approved
( ) Distribution limited to government departments and agencies; further distribution only as approved
( ) Distribution limited to defence departments; further distribution only as approved
( ) Other (please specify):

12. DOCUMENT ANNOUNCEMENT (any limitation to the bibliographic announcement of this document. This will normally correspond to the Document Availability (11). However, where further distribution (beyond the audience specified in 11) is possible, a wider announcement audience may be selected.)

UNCLASSIFIED

SECURITY CLASSIFICATION OF FORM

13 ABSTRACT (a brief and factual summary of the document. It may also appear elsewhere in the body of the document itself. It is highly desirable that the abstract of classified documents be unclassified. Each paragraph of the abstract shall begin with an indication of the security classification of the information in the paragraph (unless the document itself is unclassified) represented as (S), (C), (R), or (U). It is not necessary to include here abstracts in both official languages unless the text is bilingual).

(U) In this report we present a statistical model for the signals of an acousto-optic spectrum analyzer (AOSA). Using this model, we calculate the Cramer-Rao bound for the estimation of the carrier frequency of radar signals and the performance of the peak detector estimator. We also present an algorithm for sidelobe rejection.

14 KEYWORDS, DESCRIPTORS or IDENTIFIERS (technically meaningful terms or short phrases that characterize a document and could be helpful in cataloguing the document. They should be selected so that no security classification is required. Identifiers, such as equipment model designation, trade name, military project code name, geographic location may also be included. If possible keywords should be selected from a published thesaurus, e.g. Thesaurus of Engineering and Scientific Terms (TEST) and that thesaurus identified. If it is not possible to select indexing terms which are Unclassified, the classification of each should be indicated as with the title.)

Frequency Estimation
Statistical Analysis
Acousto-Optic Spectrum Analyzer
Sidelobe Rejection
Peak Detector Estimator
Cramer-Rao Bound

UNCLASSIFIED

SECURITY CLASSIFICATION OF FORM